Supplementary Information: Seasonality, not monthly stability anomalies, organizes aerosol vertical regimes over Central Asia

Abduxoliq Ashuraliyev

July 17, 2026

Supplementary Tables

This supplementary file reports compact robustness tables and figures for the trend, classifier, vertical-regime, profile-heating, event-ensemble, latent-regime and PM-prediction claims. Full machine-readable outputs are regenerated by the analysis scripts listed in `scripts/README.md` and stored in `outputs/tables/validation/`.

Supplementary Figures

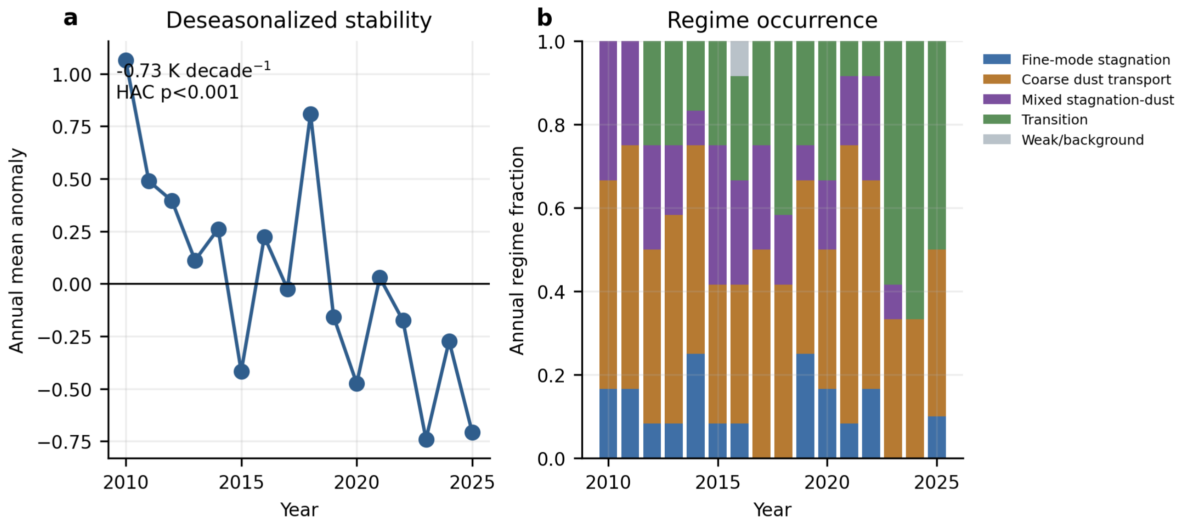

Figure S1: **Change in screened stability and aerosol-regime occurrence.** Panel (a) shows annual mean deseasonalized IGRA 700–925 hPa stability anomaly with the monthly fixed-effect HAC trend. Panel (b) shows annual fractions of the classified aerosol regimes and is descriptive only: because the classifier draws on products with time-varying coverage, regime-frequency changes are not advanced as independent trends. The 2010 and 2025 bars are partial years because the screened record begins in July 2010 and ends in October 2025.

Supplementary Trend Detail

Beyond Tables S1–S4 and the station panel (Table S15), the IGRA 700–925 hPa stability decline is confirmed by a residual 12-month moving-block bootstrap (-1.07 to -0.41 K decade^{-1}) and remains negative under residual AR(1) adjustment ($P = 7.7 \times 10^{-5}$). The station fixed-effects panel (-0.78 K decade^{-1}, all 957 station-months, station and calendar-month fixed effects) has a

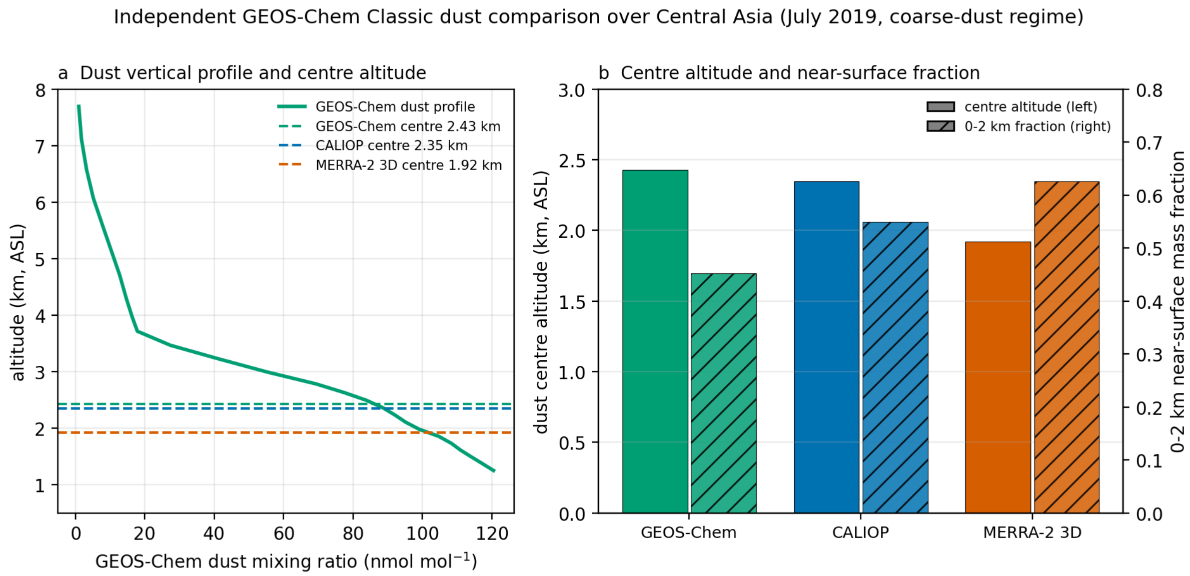

Figure S2: **Independent GEOS-Chem Classic dust comparison (July 2019, coarse-dust regime).** Panel (a) shows the domain-mean GEOS-Chem dust volume-mixing-ratio profile with the dust mass-weighted centre altitude of GEOS-Chem, CALIOP and MERRA-2 3D marked; GEOS-Chem tracks the CALIOP centre and sits above MERRA-2. Panel (b) compares the dust centre altitude (left axis) and 0–2 km near-surface mass fraction (right, hatched) across the three independent products. GEOS-Chem underestimates the dust column in this snapshot (dust AOD 0.095 versus MERRA-2 0.156 and the CALIOP-typed regional dust AOD 0.123) and simulated Dushanbe surface concentrations ($PM_{2.5}$ 18.9, PM_{10} 62.1 μg m^{-3}) preserve the dust-dominated coarse-to-fine ratio, so the run is used as a shape-and-placement check, not a burden validation.

station-clustered 95% CI of $[-1.51, -0.06]$, and the common-station panel restricted to the three $\geq$ 95%-coverage stations gives -1.09 K decade^{-1} ($[-1.56, -0.63]$); only the 69-month Urumqi record is positive and not significant. Logistic occurrence models with calendar-month controls indicate declining mixed stagnation–dust (odds ratio 0.14 decade^{-1}, FDR $q = 0.021$) and rising transition-month occurrence (odds ratio 6.17 decade^{-1}, $q = 0.0044$); classifier agreement with the default assignment is 90% (70/30 threshold), 84% (no-AERONET and no-MERRA-2), 77% (no-CALIOP) and 64% (MERRA-2-only dust proxy), so these regime-frequency trends are not advanced as independent change claims. Calendar-preserving 12-month block-permutation single-break tests place the strongest stability anomaly shift between December 2018 and January 2019 (-0.63 K, $P = 0.038$), the strongest dust-extinction anomaly shift between April and May 2017 ($+0.016$, $P = 0.023$), and the strongest mixed-regime occurrence shift between March and April 2022 (-0.20, $P = 0.004$).

Table S1: **Trend robustness for the 2010–2025 change layer.** Continuous slopes are reported in native units per decade. Regime slopes are log-odds per decade from binomial generalized linear models. HAC models include calendar-month fixed effects and 12-month Newey–West standard errors. FDR uses Benjamini–Hochberg correction across the robustness family.

Metric	HAC slope	FDR q	Theil–Sen slope	No-2010/2025 slope
IGRA 700–925 hPa stability	-0.733	1.1×10^{-5}	-0.716	-0.597
ERA5 boundary-layer height	10.615	0.021	11.923	7.626
MERRA-2 dust extinction	0.0135	0.035	0.0086	0.0129
Mixed stagnation–dust occurrence	-1.941	0.021	0.000	-1.597
Transition occurrence	1.820	0.0044	0.143	1.615

Table S2: **Classifier sensitivity against the default regime assignment.** Agreement and Cohen's κ compare each sensitivity run with the default 75/25 high/low quantile classifier over the overlapping months.

Sensitivity run	Months	Agreement	Cohen's κ
70/30 threshold classifier	184	0.902	0.858
No AERONET inputs	184	0.837	0.762
No MERRA-2 inputs	184	0.842	0.773
No CALIOP inputs	184	0.766	0.668
CALIOP-period-only subset	154	0.987	0.981
AERONET-period-only subset	121	0.942	0.916
MERRA-2-only dust proxy	184	0.636	0.496

Supplementary Methods: impact-screen assumptions

The following bounded consequence screens are locator diagnostics only; none enters the central regime, vertical-placement or transport-connectivity inference, and none is an attribution. They are summarised here for self-containment; full parameter choices and the exact numerical outputs are regenerated by the scripts in `scripts/impacts/` with outputs in `outputs/tables/impacts/`.

Same-AOD heating-placement diagnostic. Dust shortwave absorption is computed with a fixed column dust aerosol optical depth and fixed optical properties (single-scattering albedo and asymmetry parameter held constant across regimes), varying *only* the vertical distribution: the MERRA-2 dust extinction profile is replaced by the CALIOP dust-plus-polluted-dust occurrence

Table S3: **IGRA station-composition sensitivity.** The aggregate stability trend remains negative in every leave-one-station-out run. Station-level slopes vary, showing why the regional aggregate is interpreted as a screened observational index rather than a single-station climate trend.

Run	Months	HAC slope (K decade^{-1})	FDR q
Regional aggregate	184	-0.733	1.1×10^{-5}
Leave out Urumqi	184	-0.789	3.3×10^{-7}
Leave out Karaganda	184	-0.801	2.4×10^{-6}
Leave out Zhezkazgan	184	-0.700	7.9×10^{-4}
Leave out Almaty	184	-0.813	2.4×10^{-6}
Leave out Kyzylorda	184	-0.563	1.6×10^{-4}
Leave out Taraz	184	-0.551	1.8×10^{-5}

Table S4: **Product-period sensitivity for the change layer.** The stability trend remains negative in the main joined period and in the CALIOP, AERONET and post-2015 subsets. MERRA-2 dust and ERA5 BLH have consistent HAC signs but weaker AR(1) support. MODIS rows use the full March 2000–October 2025 extracted product.

Period and metric	n	HAC slope decade^{-1}	AR(1)-adjusted P
Joined 2010–2025, IGRA stability	184	-0.733	7.7×10^{-5}
CALIOP overlap, IGRA stability	156	-0.689	0.002
AERONET overlap, IGRA stability	150	-0.596	0.018
Post-2015, IGRA stability	130	-0.656	0.077
Joined 2010–2025, ERA5 BLH	184	10.615	0.052
Joined 2010–2025, MERRA-2 dust extinction	184	0.0135	0.159
MODIS 2000–2025, Tien Shan snow-pixel albedo	308	-0.0085	0.007

Table S5: **CALIOP dust-plus-polluted-dust vertical occurrence by hand-built regime.** Values are normalized detection-occurrence metrics, not extinction-profile mass integrals. Confidence intervals are bootstrap 95% intervals for regime means.

Regime	n	Center altitude (km)	95% CI	0–2 km fraction	95% CI	Above-BLH fraction
Fine-mode stagnation	17	1.692	[1.597, 1.795]	0.759	[0.732, 0.785]	0.948
Coarse dust transport	72	2.260	[2.211, 2.315]	0.594	[0.584, 0.605]	0.850
Mixed stagnation–dust	32	1.796	[1.701, 1.898]	0.728	[0.699, 0.755]	0.937
Transition	33	2.031	[1.933, 2.126]	0.652	[0.627, 0.680]	0.869

Table S6: **MERRA-2 3D minus CALIOP vertical-profile diagnostics.** CALIOP values are normalized dust-plus-polluted-dust detection occurrence; MERRA-2 values are normalized 0–15 km dust burden. The overlap score is $\sum_z \min(p_{\mathrm{CALIOP}}, p_{\mathrm{MERRA2}})$.

Regime	n	Overlap score	Center-height bias (km)	0–2 km fraction bias
Fine-mode stagnation	17	0.929	-0.084	-0.018
Coarse dust transport	72	0.914	-0.033	0.005
Mixed stagnation–dust	32	0.921	-0.044	-0.025
Transition	33	0.904	-0.165	0.028

Table S7: **Same-AOD profile-heating sensitivity.** Values are CALIOP-constrained minus MERRA-2-native diagnostic differences, using the same monthly MERRA-2 dust AOD and fixed dust optical assumptions. Negative absorption-center values mean the CALIOP occurrence profile places shortwave absorption lower than the MERRA-2 dust-burden profile.

Regime	n	Absorption-center shift (km)	0–2 km heating-fraction shift	Max heating-rate shift (K day^{-1})
Fine-mode stagnation	17	-0.308	0.018	0.0006
Coarse dust transport	72	-0.233	-0.005	0.0003
Mixed stagnation–dust	32	-0.340	0.025	0.0008
Transition	33	-0.133	-0.028	-0.0025

Table S8: **Top-10 event ensemble diagnostics (non-circular selection).** Event classes are ranked using *only* meteorology and column-aerosol variables (regional dust extinction and AOD, ERA5 boundary-layer height and 10 m wind, lower-tropospheric stability and AERONET fine-mode fraction); CALIOP vertical structure, surface PM and trajectory residence are withheld from selection. The vertical and PM columns below are therefore independent withheld-outcome associations (see Table S12). PM values are available only where OpenAQ city-month data overlap the event month.

Event class	Months	Center altitude (km)	0–2 km fraction	Above-BLH fraction	$PM_{2.5}$ anomaly (μg m^{-3})
Elevated dust transport	10	2.338	0.567	0.836	-0.8
Mixed dust-pollution	10	1.756	0.742	0.950	-20.6
Near-surface stagnation	10	1.627	0.778	0.956	26.3

Table S9: **Latent anomaly-regime model selected by BIC.** Gaussian mixtures were fit to calendar-month anomalies of the core meteorological and aerosol variables. The three-component model has the lowest BIC among two through seven components.

Latent regime	Months	Mean posterior	Stability anomaly (K)	BLH anomaly (m)	Dust extinction anomaly
Fine-stagnation anomaly	4	1.000	0.425	-78.761	-0.0375
Ventilated dust anomaly	80	0.890	-0.087	-1.291	0.0060
Weak-aerosol anomaly	100	0.896	0.054	4.243	-0.0034

Table S10: **Cross-validated $PM_{2.5}$ prediction scores.** Regression uses the fold-local target (held-out year: training-year anomaly; held-out city: absolute $PM_{2.5}$, since a new city has no training climatology); classification predicts the monthly-mean 15 μg m^{-3} severity screen (the numerical value of the WHO 2021 24-hour guideline applied to a monthly mean—a severity level, not a 24-hour-exceedance metric). Negative RMSE change means improvement relative to aerosol columns alone; paired bootstrap intervals are in Table S13. All imputers, scalers and the target normalization are fitted strictly within each training fold. The hand-built aerosol-regime label and the GMM latent-regime posterior enter as transductive covariates: they are fit once on the full covariate record (aerosol, vertical and meteorological anomalies) and are never recomputed per fold, but because they are constructed without any use of the $PM_{2.5}$ outcome they cannot leak the target. The year-held-out evaluation is nonetheless transductive with respect to atmospheric covariate construction; the primary city-held-out test holds out an entire city rather than a temporal covariate period and is therefore unaffected.

Model	Validation	RMSE	RMSE change	AUC	AUC change
Aerosol columns	Held-out year (anomaly)	19.370	0.0%	0.887	0.000
Meteorology	Held-out year (anomaly)	18.821	-2.8%	0.918	0.031
Aerosol + met + vertical/regime	Held-out year (anomaly)	18.725	-3.3%	0.919	0.032
Aerosol columns	Held-out city (absolute PM)	24.369	0.0%	0.653	0.000
Meteorology	Held-out city (absolute PM)	23.014	-5.6%	0.701	0.048
Aerosol + met + vertical/regime	Held-out city (absolute PM)	22.703	-6.8%	0.681	0.028

Table S11: **Above-boundary-layer regression is a circular specification (not interpreted).** Adjusted R^2 (HAC(12), $n = 154$) for three monthly-anomaly vertical outcomes under four predictor sets. The two outcomes defined independently of any predictor (center altitude, near-surface fraction) are unpredictable ($R^2 \leq 0.014$). The fraction above the ERA5 boundary-layer height appears predictable by meteorology (0.726) only because boundary-layer height enters both the response and the predictors; dropping it collapses the skill to 0.075. We therefore do not interpret the above-BLH regression.

Vertical outcome (monthly anomaly)	AOD only	Meteorology, no BLH	Meteorology (with BLH)	Meteorology + AOD
Center altitude	0.014	−0.011	−0.014	0.004
Near-surface 0–2 km fraction	0.013	−0.012	−0.014	0.004
Fraction above ERA5 BLH (circular)	0.039	0.075	0.726	0.740

Table S12: **Withheld-outcome significance for the non-circular event classes.** Elevated-minus-stagnation differences in outcomes never used for selection, with a month-resampling bootstrap 95% CI on the difference and a permutation p-value (outcome values shuffled across the 154-month candidate pool, 20,000 draws).

Withheld outcome	Elevated	Stagnation	Difference (95% CI)	Permutation P
Center altitude (km)	2.338	1.627	0.71 [0.54, 0.88]	$< 10^{-4}$
Near-surface 0–2 km fraction	0.567	0.778	−0.21 [−0.26, −0.16]	$< 10^{-4}$

Table S13: **Paired bootstrap intervals for the $PM_{2.5}$ prediction improvement** (full model versus aerosol columns), under strictly fold-local outcome normalization. The anomaly climatology is estimated from training data only; year-blocked uses each city's training-year calendar-month climatology, and city-held-out predicts absolute $PM_{2.5}$ (a new city has no training climatology, so this is a fully out-of-city test). With only four cities we report an observation-level and a conservative city-block bootstrap.

Validation (leakage-free target)	% improvement	Obs-bootstrap 95% CI	City-block 95% CI	$P(\Delta > 0)$ obs/city
Held-out year (train-year anomaly)	3.3	[−1.2, 7.5]	[0.2, 5.9]	0.92 / 0.996
Held-out city (absolute PM, out-of-city)	6.8	[1.5, 11.7]	[1.6, 11.0]	0.99 / 0.996

Table S14: **Null benchmarks for the CALIOP–MERRA-2 vertical overlap.** Histogram-intersection overlap of normalized 4-bin profiles ($n = 154$). The seasonality-preserving within-calendar-month shuffle is the decisive null: the matched value barely exceeds it, and MERRA-2 matches individual CALIOP months less well than the CALIOP calendar-month climatology, so MERRA-2 shows no month-specific skill beyond climatology.

Benchmark	Overlap	Interpretation
Matched month (real)	0.915	MERRA-2 vs same CALIOP month
Within-calendar-month shuffle	0.910	seasonality-preserving null ($P(\text{null} \geq \text{real}) < 10^{-3}$; excess only 0.005)
Unrestricted shuffle	0.870	destroys seasonality (conflates seasonal + monthly)
CALIOP calendar-month climatology (leave-one-year-out)	0.962	seasonal reference; beats MERRA-2
Trivial all-0–2 km profile	0.652	structural floor

Table S15: **Station-composition and dependence-robust inference for the stability trend.** Because the network grows from four to six stations within the window, we control composition explicitly and report inference robust to serial and cross-sectional dependence. The wild-cluster bootstrap clusters by station with Rademacher (±1) weights, imposes the null (restricted residuals from the model dropping t), re-estimates a station-clustered t-statistic on each of 2000 resamples, and reports the two-sided bootstrap p-value; this is the safest choice with only six clusters.

Model	n	Slope (K decade^{-1})	Inference
Station fixed-effects panel	957	−0.783	HAC [−1.13, −0.43]; station-cluster [−1.51, −0.06]; wild-cluster $P = 5 \times 10^{-4}$
Common-station panel (≥ 95% coverage)	551	−1.092	HAC [−1.56, −0.63]
Per-station: Karaganda	184	−0.350	$P = 0.032$
Per-station: Zhezkazgan	183	−0.717	$P = 8 \times 10^{-8}$
Per-station: Almaty	168	−0.364	$P = 0.087$
Per-station: Kyzylorda	169	−0.593	$P = 0.003$
Per-station: Taraz	184	−2.222	$P = 2 \times 10^{-8}$
Per-station: Wulumuqi (69 mo)	69	+0.783	$P = 0.42$ (not significant)

Table S16: **Transport connectivity versus native-emission-weighted passive-tracer arrival at Dushanbe (GEOS-Chem, July 2019).** Uniform-flux tracers give transport connectivity (similar to the HYSPLIT ensemble within two percentage points, despite different sampling periods); the native-emission-weighted run emits each tracer with GEOS-Chem's own spatially resolved dust emission flux and gives the native-emission-weighted passive-tracer arrival. Both agree the two north-western arid sectors together supply more than 99% of the tagged arrival from the four predefined regions; the split between them depends on weighting (transport geometry favours Karakum–Kyzylkum, the actual emission field favours the Aral–Caspian corridor) and is not tightly resolved at 4° × 5°.

Source region	GC connectivity (%)	HYSPLIT connectivity (%)	GC native-emission-weighted arrival (%)
Aral–Caspian dust corridor	32.6	33.4	77.1
Karakum–Kyzylkum lowlands	64.7	66.5	22.8
Iran–Afghanistan plateau	2.0	0.0	0.1
Tarim/Taklamakan sector	0.8	0.1	0.0

Table S17: **Source-region boxes and native-emission-weighted arrival robustness.** Boxes match the HYSPLIT source assignment; a grid cell is assigned to the first matching box in the listed priority order. "Cells" is the number of 4° × 5° emitting cells; the Aral–Caspian native emission is dominated by a single coarse grid cell containing the Aralkum region (79% of its regional emission), which lies on the shared Aral/Karakum boundary; the split is temporally stable across the simulated days (day-by-day below) but hinges entirely on how the two 42°N boundary cells are assigned (boundary-reassignment sensitivity quantified below).

Source region (priority order)	Lon range (°E)	Lat range (°N)	4° × 5° cells
Aral–Caspian dust corridor	58–70	42–48	6 (max cell 42°N, 60°E = 79% of emission)
Karakum–Kyzylkum lowlands	55–68	35–42	4
Iran–Afghanistan plateau	60–75	25–35	12
Tarim/Taklamakan sector	75–90	35–45	8
Day-by-day native-emission-weighted arrival (Aral–Caspian / Karakum–Kyzylkum, %):			
2019-07-03	73.1 / 26.8		
2019-07-04	75.3 / 24.6		
2019-07-05	77.1 / 22.8		
Boundary-reassignment sensitivity (Aral–Caspian / Karakum–Kyzylkum, day 2019-07-05):			
Spec A: 42°N,60°E & 65°E → Aral	77.1 / 22.8 (two-basin 99.9%; Iran+Tarim 0.1%)		
Spec B: same two cells → Karakum	2.1 / 97.8 (two-basin 99.9%; Iran+Tarim 0.1%)		
Tagged-source closure (fifth rest-of-domain tracer):			
Four source boxes	95.5% of near-surface tagged arrival at Dushanbe		
Rest of domain	4.5%		

Table S18: **Instrument-independence: event classes re-ranked with NO CALIOP input.** Classes are ranked using strictly non-CALIOP variables (MERRA-2 dust extinction, AERONET coarse-mode AOD, ERA5 boundary-layer height and 10 m wind, IGRA stability, AERONET fine-mode fraction). The withheld CALIOP vertical separation survives, so it does not arise from selection and validation sharing the CALIOP product family. Permutation p from shuffling the outcome across the 154-month pool (20,000 draws).

Withheld CALIOP outcome	n elevated / stagnation	Elevated	Stagnation	Difference (P)
Center altitude (km)	10 / 9	2.302	1.588	0.714 ($< 10^{-4}$)
Near-surface 0–2 km fraction	10 / 9	0.584	0.787	−0.203 ($< 10^{-4}$)

profile for the same regime. The absorption-weighted centroid altitude is compared between the two profiles. Holding AOD and optics fixed isolates the effect of vertical placement alone; the screen reports a downward shift of the absorption centre of 0.13–0.34 km across regimes. It is not a radiative-transfer calculation.

Population-weighted PM relative-risk and attributable-mortality screens. City populations are taken from GHSL 2025 within 10–50 km buffers around each city centre; baseline mortality uses World Bank national crude death rates; relative risk is log-linear at 1.04–1.12 per 10 μg m^{-3} applied to monthly-mean $PM_{2.5}$. The screens are neither age- nor cause-structured and use national (not city) baseline rates, so they locate where exposure is highest rather than estimating attributable burden.

MODIS snow-darkening screen. MODIS MCD43A3 albedo and MOD10A1/MYD10A1 snow cover (Google Earth Engine) are used to relate pixel-scale albedo reductions to dust loading over the surrounding mountains. This is a first-order empirical association, not a SNICAR-class snow-radiative-transfer calculation, and does not prescribe impurity optical properties.

CERES/MODIS clear-sky closure. CERES EBAF clear-sky top-of-atmosphere fluxes are used only as an observed radiative benchmark for a first-order clear-sky closure check; CERES is not used to infer aerosol forcing.

Supplementary methods detail

Within-season stability–fine-fraction correlations. Deseasonalized within-season Dushanbe fine-fraction relations to regional stability are not significant in DJF ($n = 26$, $r = -0.290$, 95% CI $[-0.639, 0.157]$, AR(1)-adjusted $P = 0.198$) or JJA ($n = 34$, $r = -0.203$, $[-0.514, 0.154]$, $P = 0.261$), moderately positive in MAM ($n = 27$, $r = 0.418$, $[0.045, 0.689]$, $P = 0.030$) and strong only in SON ($n = 34$, $r = 0.796$, $[0.602, 0.902]$, $P = 4.1 \times 10^{-7}$).

Trajectory screening configurations. The kinematic case-study and screening trajectories that are not part of the quantitative GDAS1 ensemble were run as follows. For the November 2019 case, ERA5 pressure-level winds over 20–55°N, 25–100°E drove five-day back trajectories from Dushanbe at 850, 700 and 500 hPa (six-hour steps); NOAA READY/HYSPLIT archive trajectories for November 2019 and the May 2022 top mountain-deposition month used HYSPLIT v5.4.2a, GFS0.25 meteorology, 120 h backward duration, model vertical velocity and 500/1500/3000 m AGL start heights. The ERA5 monthly-mean ranked-target ensemble integrated five-day back trajectories for 95 ranked targets at 925, 850, 700 and 500 hPa, nine start locations within ±0.5° of Dushanbe and 3-, 5- and 7-day durations; the full-period residence climatology applied the same perturbation design to all 184 classified months. Source regions used fixed Central Asian sector boxes, and trajectories leaving the extracted ERA5 domain were clipped to the nearest edge and flagged in the output table.

Supplementary reproduction commands

The exact ordered commands that regenerate every reported value, table and figure (run from the repository root; scripts are documented in `scripts/README.md`):

```
py -3 -X utf8 scripts/analysis/process_near_space.py
py -3 -X utf8 scripts/analysis/atmospheric_analysis.py
py -3 -X utf8 scripts/analysis/validation_analysis.py
py -3 -X utf8 scripts/analysis/aerosol_regime_analysis.py
py -3 -X utf8 scripts/analysis/regime_change_analysis.py
py -3 -X utf8 scripts/download/download_merra2_3d_dust_profiles.py
py -3 -X utf8 scripts/analysis/vertical_regime_diagnostics.py
py -3 -X utf8 scripts/analysis/latent_regime_model.py
py -3 -X utf8 scripts/analysis/pm_prediction_validation.py
py -3 -X utf8 scripts/impacts/vertical_profile_radiative_sensitivity.py
py -3 -X utf8 scripts/analysis/event_ensemble_diagnostics.py
py -3 -X utf8 scripts/download/download_openaq_pm.py
py -3 -X utf8 scripts/impacts/openaq_exposure_screening.py
py -3 -X utf8 scripts/impacts/population_health_screening.py
py -3 -X utf8 scripts/impacts/epidemiological_attribution.py
py -3 -X utf8 scripts/download/download_merra2_deposition.py
py -3 -X utf8 scripts/impacts/deposition_regime_analysis.py
py -3 -X utf8 scripts/impacts/modis_snow_albedo_analysis.py
py -3 -X utf8 scripts/impacts/pixel_snow_darkening_screening.py
py -3 -X utf8 scripts/impacts/ceres_regime_analysis.py
py -3 -X utf8 scripts/impacts/radiative_closure_screening.py
py -3 -X utf8 scripts/impacts/snow_impurity_radiative_transfer.py
py -3 -X utf8 scripts/trajectories/trajectory_validation.py
py -3 -X utf8 scripts/trajectories/hysplit_ready_validation.py
py -3 -X utf8 scripts/trajectories/select_source_attribution_targets.py
py -3 -X utf8 scripts/trajectories/era5_target_month_footprints.py
py -3 -X utf8 scripts/trajectories/era5_ensemble_source_attribution.py
py -3 -X utf8 scripts/trajectories/era5_full_period_residence_climatology.py
py -3 -X utf8 scripts/download/download_cams_eac4_dust_profiles.py
py -3 -X utf8 scripts/analysis/cams_vertical_bias_analysis.py
py -3.12 -X utf8 scripts/download/download_caliop_l2_daily_curtains.py
py -3 -X utf8 scripts/analysis/caliop_l2_daily_curtain_analysis.py
py -3 -X utf8 scripts/download/download_who_mortality_epidemiology_inputs.py
py -3 -X utf8 scripts/impacts/full_epidemiological_attribution.py
py -3 -X utf8 scripts/impacts/full_snow_radiative_transfer.py
py -3 -X utf8 scripts/trajectories/hysplit_ensemble_source_attribution.py
py -3 -X utf8 scripts/impacts/geoschem_dust_comparison.py
py -3 -X utf8 scripts/impacts/make_geoschem_tagged_dust_emissions.py
py -3 -X utf8 scripts/impacts/geoschem_tagged_dust_attribution.py
py -3 -X utf8 scripts/impacts/make_geoschem_native_dust_emissions.py
py -3 -X utf8 scripts/impacts/geoschem_native_dust_attribution.py
py -3 -X utf8 scripts/impacts/geoschem_tagged_closure.py
py -3 -X utf8 scripts/analysis/radiosonde_trend_homogeneity.py
py -3 -X utf8 scripts/analysis/caliop_merra2_overlap_null_benchmark.py
py -3 -X utf8 scripts/analysis/event_withheld_outcome_significance.py
py -3 -X utf8 scripts/analysis/event_no_caliop_sensitivity.py
py -3 -X utf8 scripts/trajectories/full_source_attribution_pipeline.py
```

```
py -3 -X utf8 scripts/figures/make_validation_figures.py
py -3 -X utf8 scripts/figures/make_hysplit_source_figure.py
py -3 -X utf8 scripts/figures/make_geoschem_dust_figure.py
py -3 -X utf8 scripts/figures/make_geoschem_tagged_source_figure.py
```